Active Optical Signal Conditioning and Monitoring System

Kalipada Chatterjee
Indian Institute of Technology Bhubaneswar
Subrat Sahu
Indian Institute of Technology Bhubaneswar
Venugopal Arumuru
Indian Institute of Technology Bhubaneswar
Rajan jha (rjha@iitbbs.ac.in)
Indian Institute of Technology Bhubaneswar

Article

Keywords:

Posted Date: March 1st, 2022

DOI: https://doi.org/10.21203/rs.3.rs-1134446/v2

Active Optical Signal Conditioning and Monitoring System

Kalipada Chatterjee[1], Subrat Sahu[1], Venugopal Arumuru[2], and Rajan Jha[1*]

[1]Nanophotonics and Plasmonics Laboratory, School of Basic Sciences, Indian Institute of Technology Bhubaneswar, Bhubaneswar-752050, Odisha, India.

[2]Applied Fluids Group, School of Mechanical Sciences, Indian Institute of Technology Bhubaneswar, 752050, India.

*rjha@iitbbs.ac.in

Abstract:

An optical signal conditioning technique for dynamic modulation of signals and real-time monitoring of events is pivotal for developing various optical systems at micro/nano dimensions. The utilities of such technique include controllable signal enhancement and distinctive response towards external stimuli, with reconfigurable operational range. Here, we propose and demonstrate an optical technique based on the parallel integration of fiber modal interferometers for optical response enhancement and multi-signal monitoring. Overlap of the interferometers' characteristic spectra facilitates controllable signal filtering, attenuation, and amplification of interferometer's response towards dynamic field over wide frequency range of 1 Hz – 1 kHz. Signal to noise ratio (SNR) enhancement of 9 dB is achieved by applying 1 volt about the reference interferometer. The system enables real-time modulation of optical signals and multipoint signal monitoring using machine learning for various applications such as mechanical vibrations, acoustic fields, biological samples, fluid movement, and other similar dynamic fields.

Introduction:

Optical signal modulation has gained significance to boost the development of all-optical systems for on-field real-time applications. It primarily involves spectral and/or temporal resolution, amplitude modulation, and signal enhancement by improving SNR. Such techniques have been rendered as an integral part of ultrafast communication systems[1–3], system non-linearity compensation[4], fast switching applications[5], and optical detection and monitoring systems[6–9]. With an ever-growing demand for versatile optical systems, enhancement and tuneability of response signals using passive signal processing techniques have gained importance[10,11], wherein the received signal is improved during post processing.

Among the various optical systems, optical sensing systems have become significantly viable and are prominently being developed with specialty waveguides and processed waveguides[12–18]. Although the functionalities of optical sensing systems are worthwhile in terms of sensitivity, range of operation, reconfigurability, and various parameter monitoring, yet their performance is influenced by measurand field uniformity and external disturbances. Further, optical detection systems have been extended for distributed sensing with distinct signal processing techniques[19,20] for various applications. Consequently, such systems require active optical signal modulation to reinforce their utility. The functionality of most active optical signal conditioning systems are centralized on spatial processing of sensor responses in multiparameter optoelectronic probes[21] and on signal amplitude modulation. However, along with amplitude modulation, active signal enhancement by noise filtering and localization are of paramount importance for distributed and remote dynamic field monitoring over a broad operational range. Signal enhancement using metamaterial devices[22], dimensional image restoration technique[23], additional interferometers[4], and plasmonic layers[8] have proven to be competent methods. However, these optical systems utilize expensive instrumentation and are primarily restricted to signal enhancement without providing any scope for signal attenuation

that offers utility in meeting the threshold limits of subsequent components. Besides, tuning high-frequency dynamic signals in real-time with imaging techniques would require complex systems. Comprehensive optical signal conditioning systems have been realized[24] to modulate the response of optical systems. Active[25] and passive[26] optical signal filtering techniques have been developed that require multiple expensive and customized components with operational range limitations. Hence, real-time active modulation of optical signals for signal processing that involves signal amplification, attenuation, and filtering over a broad range has remained elusive.

Optical waveguide-based interferometers are of particular interest as they exhibit efficient performance suitable for a wide range of applications like light modulation[27], sensing[18], and noise cancellation[28]. Lately, versatile fiber interferometer has been realized by using photonic crystal fiber (PCF) or speciality fiber[29–32]. Such speciality fiber-enabled interference gives additional degrees of freedom to make reconfigurable interferometers by altering the length of PCF, splicing collapsed length, and by immobilizing the surface and PCF voids with nanomaterials, gases, and liquids integrated with opto-fluidics as per the user's requirements[33,34]. The excitation of higher-order modes in PCF modal interferometer can be largely controlled to tailor the period, visibility, & uniformity of the interference pattern that modifies the interferometer response towards different external perturbations.

Here, we propose and demonstrate parallelly combined identical modal interferometers (MI) based on PCF configurations for real-time signal conditioning over a broad frequency range and SNR values. The similarity in the parallelly combined interferometers' parameters enable overlap of characteristic spectra for real-time optical signal modulation and monitoring of dynamic fields. One arm of the interferometers system is used to sense and monitor real-time dynamic fields. The signal modulation is achieved by applying a controllable equivalent dynamic field on the other MI that act as a reference. We demonstrate active controllable

amplification, attenuation, and filtering of dynamic optical response. Subsequently, we demonstrate multipoint monitoring of dynamic fields using the proposed interferometer system wherein effective signal processing techniques by machine learning are utilized for accurate signal localization.

Results and discussion

Parallel modal interferometers: The functionality of a modal interferometer relies on excitation and recoupling of speciality waveguide modes with broad spectral composition. In this work, modal interference of solid-core photonic crystal fiber (SCPCF) modes is enabled by splicing a small section of it with a single-mode fiber (SMF) channel and combining the interferometers in parallel configuration (fig.1(a)). One interferometer acts as the sensing arm (SA) while the other acts as the reference arm (RA). For individual interferometers, when SMF is fusion spliced with SCPCF, cladding voids collapse under arc heat about the spliced junctions forming regions of uniform refractive index called the collapse regions. When a broad spectral light beam is coupled to the SCPCF section via SMF, the light diffracts at the first collapse region and broadens up to the SCPCF distinct core region (fig.1 (b)). Diffraction of the otherwise guided beam causes excitation of higher-order SCPCF modes along with the fundamental mode with different propagation constants (β) as the effective indices of the higher-order mode (n_e), and the fundamental mode (~ core refractive index (n_1)) are different. If the length of collapsed region ~200 μm, the excited modes are likely to possess azimuthal symmetry such that the HE_{11} core mode and the quasi-HE_{22} (cladding mode) type modes are excited[35]. These modes overlap about the length of SCPCF (L), and coupling of modes occurs. Modal coupling is influenced by mode coupling coefficient (κ) value that is dependent on the effective modal index difference ($\Delta n = n_1 - n_e$), and spectral composition (λ) as κ is given as[36]

$$\kappa\,(\Delta n, \lambda) = \frac{\lambda}{2\pi n_1 a^2}\frac{(n_1^2 - n_e^2)}{(n_1^2 - n_2^2)}\frac{K_o(x)}{K_1^2(x)} \qquad (1)$$

where, a is the core radius, n_1 and n_2 are the effective refractive indices of the fiber core and cladding, $K_\rho^q(x)$ is the modified Bessel function of order ρ, and x is a function of $(n_e^2 - n_2^2)$ and a. At the second collapse region, the spectral components for which $\kappa(\lambda)$ values satisfy the mode coupling condition $\kappa L = m\pi$ (constructive), are coupled to the fundamental guided mode while the components for which $\kappa(\lambda)$ values satisfy the condition $\kappa L = m\pi/2$ (destructive) are coupled to the higher-order mode and become lossy. Here, m takes integer values such that m =1,2,3, … and Δn is considered to be constant as it depends on the collapsed region length. As a result, the transmission spectrum for each modal interferometer through the SMF has peaks and dips about certain wavelength values (fig.1(c)) over the source spectrum. This spectral distribution resulting from modal overlapping has an effective propagation constant ($\widetilde{\beta}_\iota$) and is referred to as the interference spectrum whose features can be controlled by configuring the lengths of interferometer and collapse region. A schematic representation of the modal interferometer is provided in **Supplementary Figure 1**. Due to the diffraction of light at the collapse region and insertion losses[37] there is a finite decrease in transmitted power. However, the transmitted spectrum is stable, temperature tolerant, and acts as a guiding spectrum for sensing applications[38–42].

On combining such identical in-line modal interferometers parallelly, it operates coherently to facilitate interactive modulation of each interferometer response. The measure of identicalness of the two interferometers' spectra is quantified by the similarity in the free spectral range (FSR) and fringe contrast (FC) of each interferometers' spectrum. In the proposed system, two identical modal interferometers are fabricated with similar values of FSR and FC. The SCPCF used as modal interferometers have a solid core of diameter 8 μm surrounded by a holey cladding with 2D photonic pattern. The length of each interferometer is chosen to be 12 ± 0.1 mm to obtain a moderate FSR value, and their resultant spectrum has an interference peak of about 1550 nm to minimize propagation loss along SMF. The fusion splicing of SCPCF and

SMF with optimized splicer parameters resulted in a collapse region of length ~211 μm that causes excitation of the aforementioned waveguide modes (see Methods section for a more detailed description of interferometer fabrication). The interferometers in a parallel configuration are powered by a light source with broad-spectrum (1400 -1600 nm). The recorded spectra for each interferometer (fig.1(c)) show that the FSR and FC values of interferometers are equivalent (see Methods section for more detailed description for the data recording process).

Moreover, the spatial frequencies of the interferometers overlap with negligible intermodulation frequencies (inset fig.1(c)). This implies that each interferometer's modal composition and effective Δn_i values of the transmitted spectrum are equivalent. Thus, the phase mismatch value between the spectra of the interferometers is nearly zero, as $\Delta\tilde{\beta} = \tilde{\beta}_1 - \tilde{\beta}_2$, where $\tilde{\beta}_i$ is the effective propagation constant for interferometer 'i' and $\tilde{\beta}_i \propto \Delta n_i$. Hence, on combining the outputs of the modal interferometers, the transmitted spectra of the individual interferometers overlap, and there is efficient coupling of power between the two arms at the 50:50 coupler.

In the presence of perturbing external field about any of the interferometers, that alter its effective L (by bending) or effective Δn (by refractive index change) values, its κL values for the spectral components get modulated. Consequently, κL values satisfy the constructive and destructive mode coupling conditions for different spectral components from the initial values, resulting in a shift of the peak and dip wavelengths of the spectrum. Under the simultaneous operation of parallelly combined interferometers, the resultant shift in the spectrum is influenced by the response of each independent interferometer towards the external field. In the event of SA being subjected to a dynamic field, such that the response of the interferometer is weak or highly amplified and/or noisy, the resultant response can be controlled by applying

an equivalent dynamic field about RA. Thus, by applying a controlled dynamic field about RA the resultant signal is amplified, attenuated, or filtered due to the interactive optical modulation of the interferometers' responses as the spectra of the interferometers overlap. The proposed system has the potential to act as an optical signal conditioner for systems that implement optical fiber-based probes for monitoring real-time dynamic fields such as acoustic field, mechanical vibrations, biochemical signature in a fluid, to name a few, wherein the nature of the external field influences the response of the probe.

Optical signal modulation

To demonstrate the optical signal modulation ability of the system, the interferometers are subjected to external mechanical vibrations, and their composite optical response is observed. Light from a fiber-coupled CW broadband source is split and coupled to each interferometer arm by the 50:50 fiber coupler and subsequently combined by another similar coupler. The transmission spectrum is detected by a wavelength interrogator that enables tracking a single peak wavelength of the resultant spectrum (see Methods for a detailed description of the experimental process). The modal interferometers are mounted on piezoelectric transducers (PZT) powered by a function generator through a multi-channel piezo-controller. External mechanical vibrations of varied parameters are applied about the interferometers, and each interferometer responds independently towards the external field. When a MI is subjected to mechanical vibrations of a specific frequency, amplitude, and initial phase, it undergoes bending along its length that modulates its spectrum. Consequently, the position of the selected peak wavelength for the corresponding spectrum oscillates periodically with equivalent frequency (f), amplitude ($\Delta\lambda$), and initial phase (p) as the applied vibrations. This response of the interferometer towards the external field is considered as the optical signal. This signal of SA is modulated by controlling the equivalent field about RA that influences the resultant

spectrum. A schematic representation of the basic experimental setup is provided in **Supplementary Figure 2**.

Signal amplification: In order to demonstrate signal amplification, both interferometers are operated simultaneously. The frequency, amplitude, and initial phase of vibrations are fixed about SA. Additionally, RA is subjected to vibrations of the same frequency, initial phase, and an initial value of amplitude. The resultant signal is a sinusoidal signal of the corresponding frequency with amplitude equal to the sum of the amplitudes of the signals of interferometers. By varying the value of vibration amplitude about RA, the amplitude of the resultant signal changes. The increment in the amplitude of the resultant signal in terms of $\Delta\lambda$ (peak-to-dip) is shown in fig.2(a) with real-time signal at 100 Hz as inset. If the vibration amplitude about RA increases or decreases, the resultant amplitude increases or decreases linearly over the voltage range. The rate of increase in signal amplitude with applied voltage about RA is observed to be 7.8 pm/V at 100 Hz. Such signal amplification is similar at different field frequencies. The minimum value of amplitude for the resultant signal is equal to the amplitude of the signal in SA that is when no vibrations are applied about RA. Technically, when the SA is subjected to an external dynamic field of low amplitude, the resultant response of the system is enhanced by applying an equivalent field of a similar frequency about RA such that the combined responses have higher effective amplitude. Such ability can be utilized for enhancing the response towards low-intensity dynamic fields due to strain, any material immobilization around the interferometer, selective biochemical detection, to name a few.

Signal attenuation: Signal attenuation deals with suppressing the frequency components of the resultant signal by controlling the parameters of the dynamic field about RA. Experimentally, the frequency, amplitude, and initial phase of vibrations about SA are fixed. Mechanical vibrations of similar frequency and amplitude are applied to RA. In order to attenuate the resultant signal, the relative phase between the signals about the interferometers

is varied by changing the initial phase of vibrations about RA. As the relative phase difference between the vibrations increases, the amplitude of the resultant signal decreases reaching a minimum value for a relative phase difference of 180^{o}. The characteristic attenuation plot that has a linear nature is represented in fig.2 (b) with real-time signal in the inset. A decrement in the signal amplitude of -22 pm/degree at 100 Hz of initial phase about RA is observed. The cause is attributed to the destructive superposition of interferometers' responses that decrease the amplitude of the resultant signal. Suppose the signal amplitude of SA due to the external dynamic field is higher than a certain threshold level of the detection system. In that case, it can be attenuated by controlling the phase of RA signal. Such a technique can be used to avoid physical damages of subcomponents due to high amplitude signals by noise suppression and active harmonic filtering.

Signal Filtering: Dynamic field perturbations tend to be noisy due to several environmental and intrinsic factors. In the presence of such an external field, the response of the interferometer gets noisy with a very low signal-to-noise ratio (SNR) value that leads to analysis difficulties. In the proposed system, a noisy signal of SA is superposed by a controlled signal of RA with similar parameters to generate a resultant signal of a high SNR value. In the experimental setup, random noise is introduced in the piezo vibration signal about SA. As a result, the signal of the interferometer is noisy with a low SNR value. Subsequently, a dynamic field of equivalent frequency is applied about RA such that the signal of RA superposes with the noisy signal of SA to generate a resultant stable signal with a high SNR value. The enhancement in SNR value with change in voltage about RA is computed from the recorded data and shown in fig.2 (c) with real-time signal in the inset. By increasing the amplitude of the reference signal, the resultant signal becomes more regular. SNR enhancement of about 9 dB is achieved by applying only 1 Volt signal about the reference interferometer. The SNR values increase and get saturated at a certain value of reference signal amplitude. The saturation of SNR value is

attributed to the limit of interferometer sensitivity that depends on interferometer configuration and its positioning over PZT. Additionally, the variation in SNR values with applied field frequency is investigated over the operational range. The SNR values for different field frequencies about SA are maintained at a nearly uniform level, and then its response is superposed with the response of RA towards an equivalent field at fixed amplitude. The filtering ability of the system is analysed over the frequency range and is observed to be nearly uniform over the operational range. Such operational utility of the proposed system has the potential to improve the system's response towards low unsteady perturbing dynamic fields encountered in optoelectrical and mechanical devices, which are employed in communication and environmental monitoring systems.

Multi-point parameter monitoring

The combination of such interferometers acts as a sensing system for monitoring physical fields of varied nature. In the presence of perturbing fields about each interferometer, the resultant signal is a superposition of the signals of the individual interferometers. If the external field, irrespective of its cause, alters the effective L or effective Δn of the interferometers, the resultant signal shifts providing a distinct signature of the external field. The resultant composite signal is analysed using computational tools to scrutinize the external field.

Mechanical vibration sensing: In the event of subjecting the interferometers to a dynamic strain field, the interferometers respond independently, generating a resultant signal that has frequency components with corresponding amplitudes as that of the individual signals. Mechanical vibrations of varied frequencies are applied to each interferometer, and the resultant signals are recorded. The signal frequencies are spanned over 1 Hz-1 kHz, and various combinations of signal components are applied about the interferometers. Consequently, real-time composite signals with vibration features are recorded. The composite signals are assessed

using computational techniques for localizing the signal features about each interferometer. The continuous wavelet transform (CWT) technique is employed to derive the signal components from the composite signal and, hence, determine the individual signals' instantaneous phase. Fast Fourier transform (FFT) of the signals yields the frequencies present in the signal with their respective amplitudes. A few real-time composite signals with their corresponding instantaneous phase and FFT are provided in **Supplementary Figure 3.** The important aspect of multipoint field monitoring lies in identifying the location of individual frequency components about the interferometers from the resultant signal. The localization of the signal components for the system is achieved by a sequence of steps using the machine learning technique as represented in fig.3 (a). Firstly, CWT is used to generate the scalograms of the composite signals. The scalograms corresponding to signal combinations of 10 Hz and 20 Hz are shown in fig.3 (b) and (c). The distinct feature of the scalograms of the composite signals is the circular contours along the top horizontal direction that vary with signal combinations. These scalograms are then used as a training set to optimize a Dense Convolutional Network (DenseNet) model that includes convolutional neural networks (CNN) and deep artificial neural networks (ANN) algorithms (details are mentioned in the Methods section). The features of the scalograms are parameterized and utilized to determine the frequency components about the interferometers. The developed model for localization of the signals has an accuracy of 86%. The proposed method is versatile and can be extended for more than two interferometers combined parallelly.

Biological sample detection: To demonstrate the versatility of the proposed system, the interferometers system is tested with biological samples by exposing them to Bacillus megaterium (B.mega) samples. The interference peak wavelength is tracked, and its shift is recorded as the interferometers are exposed to biological samples. B.mega sample is prepared by culturing the bacteria in conventional nutrient broth. With an increase in the bacteria

population, the optical density (OD) and hence, the refractive index of the sample increases. As the bacteria in the sample dies, the OD and index of the sample decreases[43]. Firstly, the interferometers are exposed to the nutrient broth and live bacteria sample (cultured in broth), and the corresponding peak shifts are recorded, as shown in fig.3 (d) inset. The peak incurs a red shift in both cases as the effective Δn value increases. However, the peak shift for bacteria sample exposure is more owing to a higher OD of the sample. Subsequently, in the presence of broth environment about both interferometers, a live bacteria sample is injected about Int-1 (event-1), and subsequently, dead bacteria sample is injected about Int-2 (event-2) (details are mentioned in the Methods section). In the presence of the live bacteria sample, the interference peak wavelength incurs redshift, while as the dead bacteria sample is injected, the peak incurs a blue shift due to a lower OD value of the sample. The magnitude of the shift is depicted in fig.3(d). In a scenario where both interferometers are exposed to such a biological sample, the event of a live bacteria about Int-1 getting killed by some agent in the environment and coming in contact with Int-2 can be detected by monitoring the peak shift in real-time. Such application can be used for analysing the cell cycles and interaction of biochemical agents with microorganisms[44] in real-time. The interferometers can be immobilized to facilitate the detection of SARS viruses.

Discussion:

We report a system of modal interferometers in parallel combination to act as a comprehensive system for optical signal modulation over a broad range. With an increase in demand for optical sensing systems in real-time dynamic field monitoring, such a system offers a technique to modulate the response of optical sensing probes. The identicalness of the modal interferometers facilitates the overlap of transmission spectra to allow interactive modulation of the interferometer signals. The interferometers' features that are the lengths of interferometer and collapse region, can be reconfigured to modify the resultant transmission spectrum. The

reconfigurability nature of the modal interferometer offers scope to customize the sensitivity and range of operation of the system. Besides, the signal of SA is attenuated by varying the relative phase between the interferometer signals.

Additionally, the noisy response of SA towards an external field is filtered, resulting in enhancement of the signal by controlling the field about RA. By reconfiguring the sensitivity of the modal interferometers, their resonant frequencies can be varied to enable noise reduction in operating micro-resonators[45]. Since the RA of the system can be spatially located independently from SA, the proposed system has a wider range of controllability and applicability than reported systems.

Further, the proposed system offers a technique for multipoint monitoring of dynamic field-frequency, amplitude, and instantaneous phase over broad ranges of 1 Hz - 1 kHz using machine learning algorithms. Moreover, the system facilitates the detection of biological samples in order to distinguish between live and dead micro-organisms samples.

In summary, we report a modal interferometer-based interferometer system for the modulation of responses of optical sensors. By reconfiguring the interferometer in the RA, its transmission spectrum can be made equivalent with that of an optical probe in the SA to facilitate the modulation of the latter's response towards the external dynamic field. The multipoint sensing ability of the proposed system can be extended for more than two interferometers in parallel combinations to facilitate multiplexing. We hope the proposed system has the potential to develop an active technique for optical signal conditioning for utility in real-time applications employing optical devices.

Methods:

Modal interferometer fabrication: The SCPCF used as modal interferometer has outer diameter of 125 μm with core of diameter 8 μm, surrounded by a sixfold symmetric arrangement of voids with diameter 3.1 μm and pitch of 6.6 μm. For preparing the first SCPCF-SMF section in the SA, at first, SCPCF of length 12 ± 0.01 mm is taken whose ends are thoroughly cleaned and cleaved perpendicularly using precision fiber cleaver (Sumitomo, FC-6RS). The cleaved ends of the SCPCF are then spliced with SMFs (8/125 μm, SMF-28) at optimized parameters using a fusion splicer (Fujikura, 80S). The arc time is kept at ~3000 ms, and the arc power is STD-20 bit. The fiber cores are precisely aligned, which resulted in a collapse region of length ~ 211 μm. The modal interferometer in the RA is prepared in a similar manner such that the interferometers are identical. The FSR for each interferometer (i) is calculated as $FSR_i = \frac{\lambda_o^2}{(\Delta n_i L_i)}$ where, λ_o is the central wavelength, Δn_i is the difference between the effective mode indices and L_i is the length of the corresponding interferometer. Also, FC is obtained using $FC = -10\log(1 - v_i)$ where v_i is the corresponding visibility parameter. The length of the interferometers is kept as 12 mm so that the period of the interference pattern is broad and the peaks are sufficiently distinct to avoid overlapping. The fabricated interferometers are combined with the arms of a 1x2 coupler at both ends using FC/PC fiber connectors to be characterized experimentally.

Numerical calculations: 2D light propagation through the SMF-PCF-SMF fiber channel is simulated by finite element method using wave optics module in COMSOL Multiphysics. The parameters used for FEM simulations are scaled accurately concerning the experimental setup. The mesh element size was set to be smaller than 1/12 of the area of the fiber channel. The computation is carried to obtain two modes for the spectral range.

Experimental characterization: The proposed system is characterized to demonstrate the optical signal modulation using the fiber interferometer principle. Light from CW superluminescent light-emitting diode (SLED, Thorlabs S5FC1005S) of 10 mW is coupled to interferometers system using 1x2 3 dB coupler and combined using a similar coupler. This ensures that the path lengths of the signals from the interferometer up to the detector are equal and that the splitting and recombination of the signals occur with the same power coupling efficiency over the spectrum. Initially, the characteristic transmission spectra of each interferometer and their combination are recorded using an optical spectrum analyser (OSA, Yokogawa) shown in fig.1 (c). For signal modulation, the output of the resultant spectra is detected using an FBG based wavelength interrogator (by Ibsen) and recorded on a computer system via an ethernet interface. The interferometers are driven in a controlled manner by the PZTs driven by piezo-controllers (PiezoDrive PD200 Amplifier) to test the response of the interferometers and their interactive modulation effect. For demonstrating vibration sensing ability, various signal combinations are applied about the interferometers by controlling the vibrations of PZTs using suitable function generators. The real time-series signals are recorded using the wavelength interrogator keeping the scanning frequency and signal time duration constant for the datasets. The ability of biological sample sensing of the system is carried out in a sequential manner. Firstly, the peak shift over time due to exposure of interferometers towards bacteria nutrient broth is recorded and is considered as a reference level. B.mega bacteria is cultured in optimized conditions in the same broth. 1 ml of live bacteria sample containing ~10^6 bacteria cells are injected on Int-1 while both interferometers are partially immersed in broth solution (reference level). The corresponding shift in peak wavelength is recorded. In order to test the distinction of live and dead bacteria samples, both interferometers are partially immersed in broth solution, and live and dead bacteria samples are injected sequentially upon Int-1 and Int-2, respectively. The corresponding peak shift is recorded over

a finite time duration until the peak shift saturates. The proposed system in principle may work for a higher range of frequencies, however, due to unavailability of a high-frequency interrogator and piezo actuator, our study is restricted to 1 kHz.

Computational calculations: The composite signals of the proposed system are analysed by computational techniques using MATLAB R2020b. The absolute values of SNR of the noisy signals and the filtered signals, generated by controlling the field about the RA, are calculated by developing computational codes for signal SNR calculation in MATLAB. The SNR is calculated from the FFT of the composite signal wherein the ratio of the area under frequency component to that of the noise floor is evaluated computationally on a log scale.

The machine learning technique is implemented for the localization of interferometer signals based on a supervised technique using convolutional networks (CNN) followed by deep artificial neural network (ANN) principles. CNN enables image (scalogram) parameterization while ANN enables signal localization. The output values of the parameterization network are fed to the ANN network. The ANN network provides the output in the form of binary classification (either 0 or 1) that enables the prediction of frequency components about the interferometers. Both networks are merged via a fully connected layer, resulting in the creation of a massive network. Developing a giant model that combines CNN and ANN from scratch takes a long time and a lot of computation power. So, rather than designing a completely new CNN architecture, we adopted 121-layer Dense Convolutional Network (DenseNet), developed by Huang et al., to minimize training time and boost efficiency. With the aid of interferometers, a total of 285 signal combinations are produced. Wavelet transformation is used to convert obtained signal combinations into scalogram images. From the 285 images, 256 images are used in the training dataset, and 29 images are used to test the model's accuracy. The obtained scalograms are fed to DenseNet model. The DenseNet architecture provides 208896 parameters through fully connected layers. In the giant model, 208896 encoded

parameters acquired from CNN are provided input to the ANN network. Throughout the training of the giant network, hyperparameters, weights, and biases of CNN are kept constant. Only the hyperparameter of ANN is modified during the training period. By analysing the parameters, the ANN provides an output regarding signal localization. After optimizing the DenseNet model, it is tested with the remaining set of images to determine the model accuracy that is estimated to be 86%.

Acknowledgements:

KC thanks Dhruv Thummar for assisting in the computational formulation and signal processing and also Biswaranjan Pradhan and Neelanjana Sahu for providing necessary support for the bacteria sample culture. R.J. acknowledges the support of SERB-STAR fellowship. This work is partially supported by STR/2020/000069.

Author Contributions:

KC and SS fabricated the interferometers, conducted the experiment, carried out the simulations, and analysed the results. VA and RJ conceived ideas and provided necessary suggestions in the experimental work. KC, SS, VA, and RJ have prepared the manuscript and compiled the entire work.

Data availability

The datasets generated and/or analysed during the current study are available from the corresponding authors on reasonable request.

Corresponding author
Correspondence to: Dr Rajan Jha (rjha@iitbbs.ac.in)

Competing interests
The Optical System and Method for Active Modulation of Optical Signals presented is subject to patent filing: Indian Patent Application 202131047683.

Additional information

Supplementary Information accompanies this paper and can be found in the SI section or requested from the corresponding author(s).

References:

1. Liu, Z. *et al.* Modulator-free quadrature amplitude modulation signal synthesis. *Nat. Commun.* **5**, (2014).

2. Li, L. *et al.* All-optical regenerator of multi-channel signals. *Nat. Commun.* **8**, (2017).

3. Xomalis, A. *et al.* Fibre-optic metadevice for all-optical signal modulation based on coherent absorption. *Nat. Commun.* **9**, (2018).

4. Sutherland, H. E. & Manuel, R. M. Signal conditioning for compensating nonlinearity and nonrepeatability of an optical frequency scanning laser implemented in a C-OFDR system. *Appl. Opt. Vol. 56, Issue 3, pp. 457-461* **56**, 457–461 (2017).

5. Blumenthal, D. J. *et al.* Optical signal processing for optical packet switching networks. *IEEE Commun. Mag.* **41**, (2003).

6. Thévenaz, L., Niklès, M. & Robert, P. A. Simple distributed fiber sensor based on Brillouin gain spectrum analysis. *Opt. Lett. Vol. 21, Issue 10, pp. 758-760* **21**, 758–760 (1996).

7. Wolffenbuttel, R. F. State-of-the-art in integrated optical microspectrometers. *IEEE Trans. Instrum. Meas.* **53**, 197–202 (2004).

8. Echtermeyer, T. J. *et al.* Strong plasmonic enhancement of photovoltage in graphene. *Nat. Commun.* **2**, (2011).

9. Schmeckebier, H. & Bimberg, D. Quantum-Dot Semiconductor Optical Amplifiers for Energy-Efficient Optical Communication. in *Springer* 37–74 (2017). doi:10.1007/978-3-319-67002-7_3.

10. Liu, Y. *et al.* All-optical signal processing based on semiconductor optical amplifiers. *Front. Optoelectron. China* **4**, 231–242 (2011).

11. Li, M. *et al.* Reconfigurable Optical Signal Processing Based on a Distributed Feedback Semiconductor Optical Amplifier. *Sci. Rep.* **6**, (2016).

12. Caucheteur, C., Guo, T., Liu, F., Guan, B. O. & Albert, J. Ultrasensitive plasmonic sensing in air using optical fibre spectral combs. *Nat. Commun.* **7**, (2016).

13. Dong, Y. High-Performance Distributed Brillouin Optical Fiber Sensing. *Photonic Sensors* vol. 11 69–90 (2021).

14. Oh, J. W. *et al.* Biomimetic virus-based colourimetric sensors. *Nat. Commun.* **5**, (2014).

15. Chow, D. M., Yang, Z., Soto, M. A. & Thévenaz, L. Distributed forward Brillouin sensor based on local light phase recovery. *Nat. Commun.* **9**, (2018).

16. Sun, X. *et al.* Genetic-optimised aperiodic code for distributed optical fibre sensors. *Nat. Commun.* **11**, (2020).

17. Joe, H. E., Yun, H., Jo, S. H., Jun, M. B. G. & Min, B. K. A review on optical fiber sensors for environmental monitoring. *Int. J. Precis. Eng. Manuf. Technol. 2018 51* **5**, 173–191 (2018).

18. Zhao, P. *et al.* Mode-phase-difference photothermal spectroscopy for gas detection with an anti-resonant hollow-core optical fiber. *Nat. Commun.* **11**, 1–8 (2020).

19. Sladen, A. *et al.* Distributed sensing of earthquakes and ocean-solid Earth interactions on seafloor telecom cables. *Nat. Commun.* **10**, (2019).

20. Williams, E. F. *et al.* Distributed sensing of microseisms and teleseisms with submarine dark fibers. *Nat. Commun.* **10**, (2019).

21. Wolffenbuttel, R. F. State-of-the-art in integrated optical microspectrometers. *IEEE Trans. Instrum. Meas.* **53**, 197–202 (2004).

22. Chen, Y., Liu, H., Reilly, M., Bae, H. & Yu, M. Enhanced acoustic sensing through wave compression and pressure amplification in anisotropic metamaterials. *Nat. Commun.* **5**, (2014).

23. Soto, M. A., Ramírez, J. A. & Thévenaz, L. Intensifying the response of distributed optical fibre sensors using 2D and 3D image restoration. *Nat. Commun.* **7**, (2016).

24. Vo, Q., Fang, F., Zhang, X. & Zhu, L. Reducing the residual focus error signal in optical pickup head astigmatism displacement systems using the signal conditioning method. *Appl. Opt.* **57**, 9972 (2018).

25. Ip, E., Lau, A. P., Barros, D. J. & Kahn, J. M. Coherent detection in optical fiber systems: erratum. *Opt. Express* **16**, 21943 (2008).

26. Hu, L., Tian, X., Wu, G. & Chen, J. Passive optical phase noise cancellation. *Opt. Lett.* **45**, 4308 (2020).

27. Tzuang, L. D., Fang, K., Nussenzveig, P., Fan, S. & Lipson, M. Non-reciprocal phase shift induced by an effective magnetic flux for light. *Nat. Photonics 2014 89* **8**, 701–705 (2014).

28. Driggers, J. C., Evans, M., Pepper, K. & Adhikari, R. Active noise cancellation in a suspended interferometer. *Rev. Sci. Instrum.* **83**, (2012).

29. Zhao, J. *et al.* Lateral offset optical fiber modal interferometer sensor for simultaneous measurement of seawater temperature and salinity. *Elsevier*.

30. Du, J., Dai, Y., Lei, G. K. P., Tong, W. & Shu, C. Photonic crystal fiber based Mach-Zehnder interferometer for DPSK signal demodulation. *Opt. Express* **18**, 7917 (2010).

31. Dong, X., Tam, H. Y. & Shum, P. Temperature-insensitive strain sensor with polarization-maintaining photonic crystal fiber based Sagnac interferometer. *Appl. Phys. Lett.* **90**, (2007).

32. Rifat, A. A. *et al.* Photonic crystal fiber based plasmonic sensors. *Sensors and Actuators, B: Chemical* vol. 243 311–325 (2017).

33. Shrivastav, A. M., Sharma, G., Rathore, A. S. & Jha, R. Hypersensitive and Selective

Interferometric Nose for Ultratrace Ammonia Detection with Fast Response Utilizing PANI@SnO2 Nanocomposite. *ACS Photonics* **5**, 4402–4412 (2018).

34. Arumuru, V., Dash, J. N., Dora, D. & Jha, R. Vortex Shedding Optical Flowmeter based on Photonic Crystal Fiber. *Sci. Rep.* **9**, (2019).

35. Cárdenas-Sevilla, G. A., Finazzi, V., Villatoro, J. & Pruneri, V. Photonic crystal fiber sensor array based on modes overlapping. *Opt. Express* **19**, 7596 (2011).

36. Snyder, A. W. Coupled-mode theory for optical fibers. *J Opt Soc Am* **62**, 1267–1277 (1973).

37. Chen, J., Mikulic, P., Eftimov, T. A. & Bock, W. J. An Inline Core-Cladding Intermodal Interferometer Using a Photonic Crystal Fiber. *J. Light. Technol. Vol. 27, Issue 17, pp. 3933-3939* **27**, 3933–3939 (2009).

38. Nankali, M., Einalou, Z., Asadnia, M. & Razmjou, A. High-Sensitivity 3D ZIF-8/PDA Photonic Crystal-Based Biosensor for Blood Component Recognition. *ACS Appl. Bio Mater.* **4**, 1958–1968 (2021).

39. Khan, M. R. H., Ali, F. A. M. & Islam, M. R. THz sensing of CoViD-19 disinfecting products using photonic crystal fiber. *Sens. Bio-Sensing Res.* **33**, (2021).

40. Gao, R., Jiang, Y. & Abdelaziz, S. All-fiber magnetic field sensors based on magnetic fluid-filled photonic crystal fibers. *Opt. Lett.* **38**, 1539 (2013).

41. Teng, L. *et al.* Temperature-compensated distributed hydrostatic pressure sensor with a thin-diameter polarization-maintaining photonic crystal fiber based on Brillouin dynamic gratings. *Opt. Lett.* **41**, 4413 (2016).

42. Jha, R., Villatoro, J., Badenes, G. & Pruneri, V. Refractometry based on a photonic crystal fiber interferometer. *Opt. Lett.* **34**, 617 (2009).

43. De Leersnyder, I., De Gelder, L., Van Driessche, I. & Vermeir, P. Influence of growth media components on the antibacterial effect of silver ions on Bacillus subtilis in a liquid growth medium. *Sci. Reports 2018 81* **8**, 1–10 (2018).

44. Kohanski, M. A., Dwyer, D. J. & Collins, J. J. How antibiotics kill bacteria: From targets to networks. *Nature Reviews Microbiology* vol. 8 423–435 (2010).

45. Zhang, Q., Zhai, R., Yang, S., Yang, S. & Li, Y. Microfiber Mechanical Resonator for Optomechanics. *ACS Photonics* **7**, 695–700 (2020).

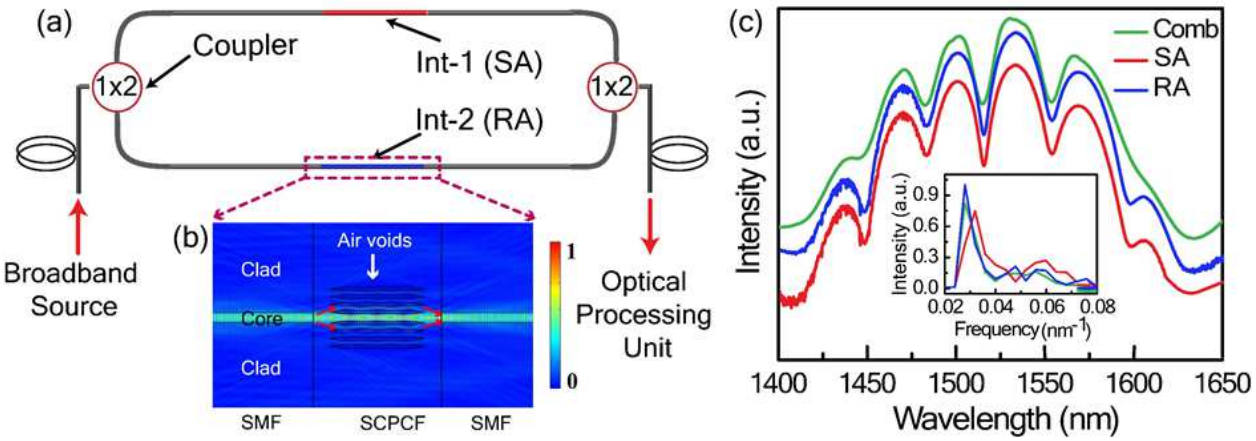

Figure 1: **Parallel Modal Interferometer:** (a) Schematic representation of the modal interferometer (MI) wherein SMF: Single mode fiber, CR: Collapse region, SCPCF: Solid core photonic crystal fiber, I/P: Input and O/P: Output. (b) FEM analysis (using COMSOL v5.5) of light beam propagation through the modal interferometer depicting the excitation and recombination of SCPCF modes about the collapse region. (c) Transmission spectra of each of the identical MI with SA: Sensing arm and RA: Reference arm and the resultant transmission spectrum (Comb) when combined parallelly. (inset) FFT of the transmission spectra of SA and RA and their combination has 0.03 nm^{-1} as the prominent spatial frequency.

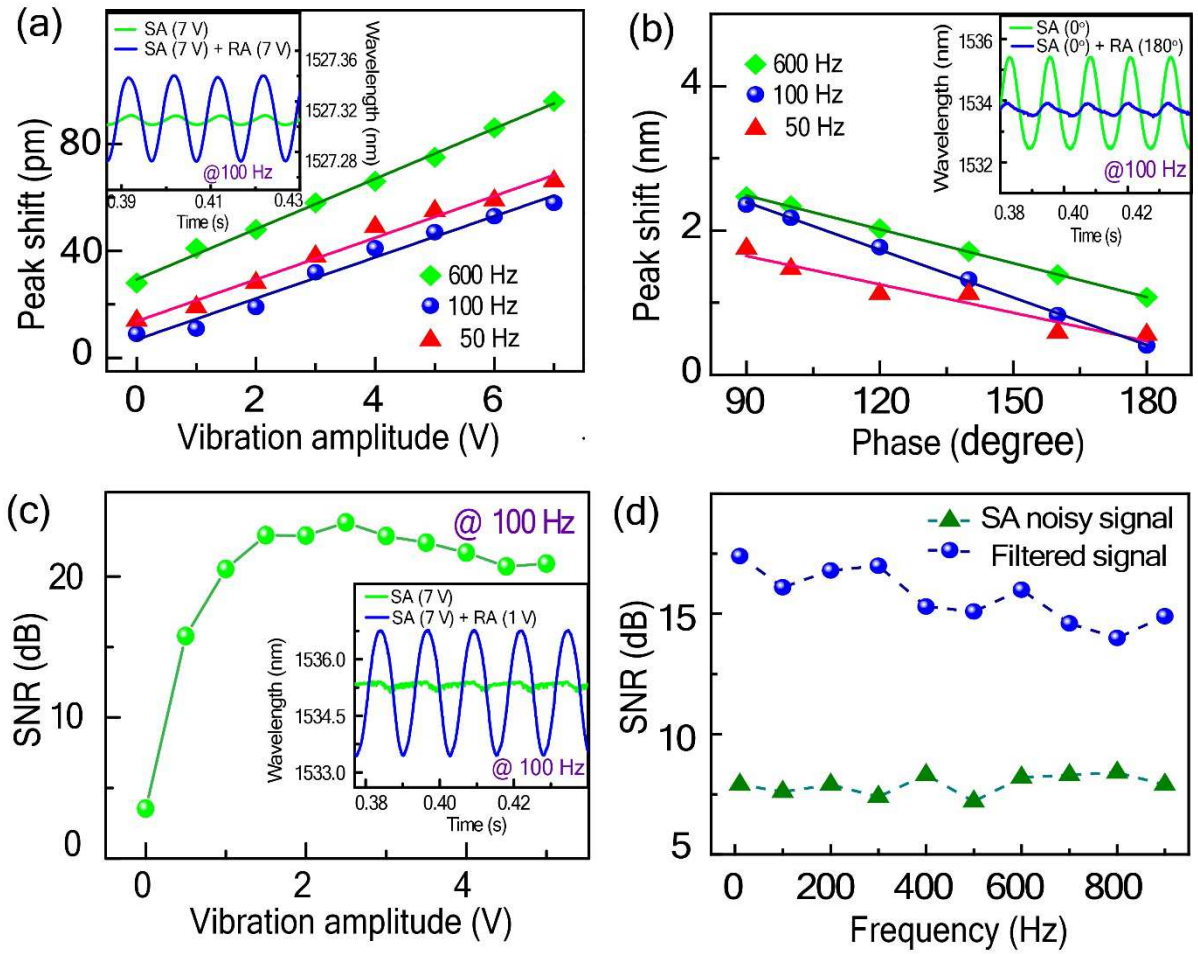

Figure 2: **Optical Signal Modulation**: (a) Signal amplification: Characteristic plot for amplification of the resultant signal with change in field amplitude about RA for varied frequencies (inset) Real time resultant transmission signal of the parallel interferometers for operating (green curve) only SA at 100 Hz and constant amplitude and then (blue curve) operating SA and RA simultaneously at 100 Hz with field amplitude of 3 V about RA. (b) Signal attenuation: Characteristic plot for attenuation of the resultant signal with change in the initial phase of the dynamic field about RA for varied frequencies. (inset) Real time resultant transmission signal of the parallel interferometers for operating (green curve) only SA at 100 Hz, constant amplitude and phase and then (blue curve) operating SA and RA simultaneously at 100 Hz, equivalent amplitudes with initial phase of signal about RA as 180°. (c) Signal filtering: Computed SNR values for the resultant signals obtained by varying the amplitude of dynamic field about RA at fixed frequency (100 Hz). (inset) (green curve) Real time response of the noisy signal of SA (field amplitude: 7 V) and (blue curve) the combined response after applying field about RA 100 Hz and 1 V. (d) (green curve) Variation of SA signal SNR with frequency while RA is inactive and (blue circles) Variation of filtered signal SNR with frequency when RA is active keeping the field frequency at 0.5 V.

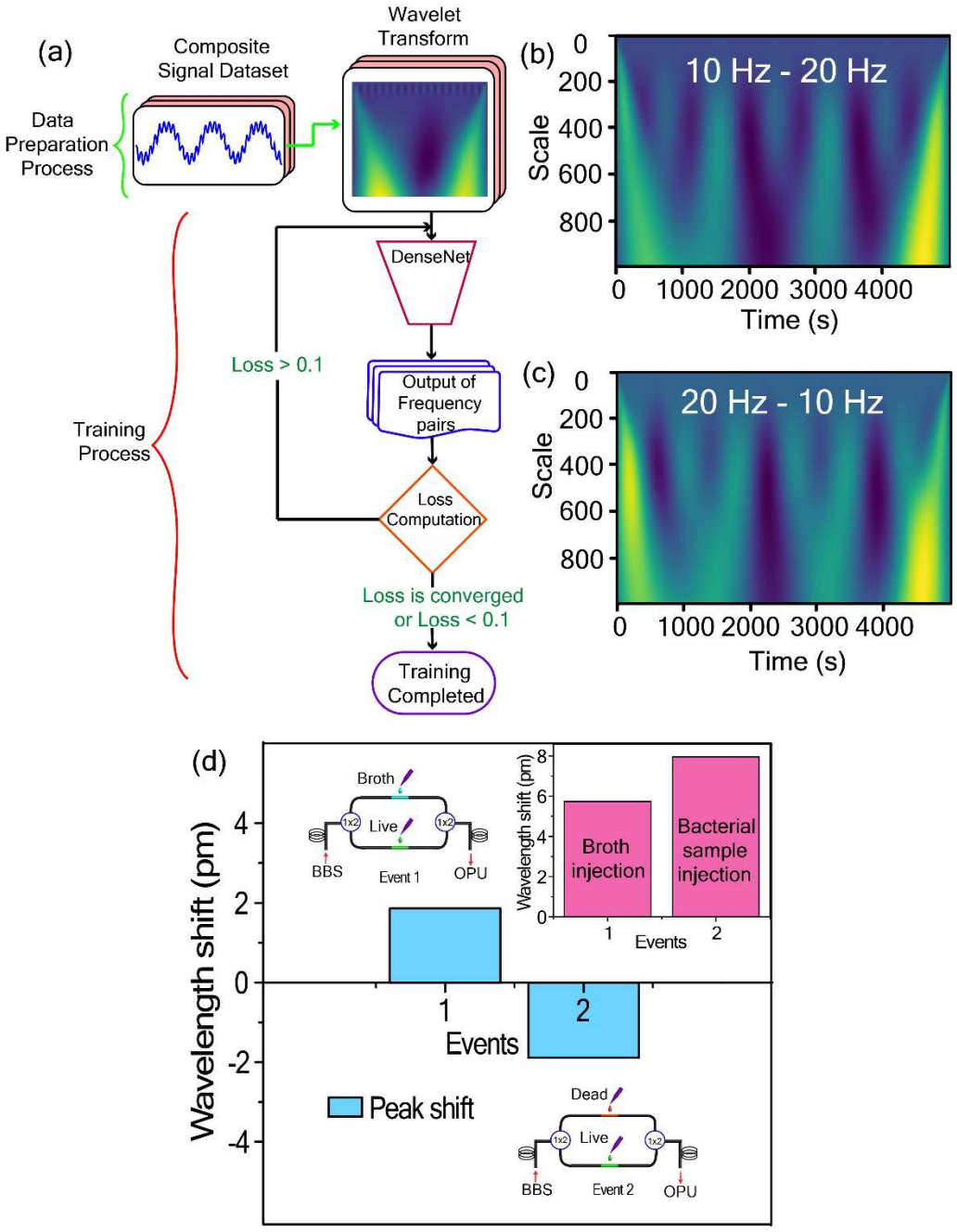

Figure 3: **Multipoint Parameter Monitoring:** (a) Mechanical vibration monitoring: Schematic representation of machine learning technique based on DenseNet architecture used for signal localization (b)&(c) Scalograms of real-time resultant signal of parallel interferometer system for operating Int-1 at 10 Hz and Int-2 at 20 Hz and vice versa, respectively. The scalograms are obtained by CWT of the real-time signals and have distinct contour features. (c) Biological sample detection: Shift in peak wavelength of interference spectrum on exposing Int-1 with live bacteria (B.mega) sample (event-1) and subsequently injecting dead bacteria (B.mega) sample upon Int-2 (event-2) while both interferometers were partially surrounded by nutrient broth. (inset) Interferometer response (peak shift) for injecting Int-1 with nutrient broth (event-1) and for injecting Int-1 with live bacteria (B.mega) sample (event-2) while Int-2 is in broth environment.

Supplementary Files

This is a list of supplementary files associated with this preprint. Click to download.

- SupplementaryInformation.docx